Research Article Vol. 30, No. 24 / 21 Nov 2022 / Optics Express 44175

Optics EXPRESS

Towards underwater quantum communication in the mesoscopic intensity regime

ALESSIA ALLEVI[1,2,*] AND MARIA BONDANI[2]

[1] Department of Science and High Technology, University of Insubria, Via Valleggio 11, I-22100 Como, Italy
[2] Institute for Photonics and Nanotechnologies, IFN-CNR, Via Valleggio 11, I-22100 Como, Italy
[*] alessia.allevi@uninsubria.it

Abstract: The problem of secure underwater communication can take advantage of the exploitation of quantum resources and novel quantum technologies. At variance with the current experiments performed at the single photon level, here we propose a different scenario involving mesoscopic twin-beam states of light and two classes of commercial photon-number-resolving detectors. We prove that twin-beam states remain nonclassical even if the signal propagates in tubes filled with water, while the idler is transmitted in free space. We also demonstrate that from the study of the nonclassicality information about the loss and noise sources affecting the transmission channels can be successfully extracted.

1. Introduction

In the field of optical quantum communication, many advances have been made during the last two decades for transmission in free space and through optical fibers. Many experiments have demonstrated that secure communication of information is possible both over long distances and at a very high rate [1]. In the last few years, a novel interest concerning the transmission of information encoded in optical states in the underwater environment has arisen, and several potential applications have been devised, such as communication between submersibles, research vessels and surface vehicles [2–5]. Previous studies have demonstrated that the maximum length of an underwater quantum channel is expected to be a few hundred meters [6] , which is very short with respect to the standard communication channels (optical fibers and free-space links) [1,7], but this could be enough for the typical communications in underwater environment [4]. Moreover, also the frequency rate at which information is transmitted is generally low (few kHz at maximum) [8]. Note that the experimental investigations on underwater quantum communications performed so far have involved the use of single-photon detectors [9] and the different degrees of freedom of the quantum states, such as polarization, transverse momentum, time-bin, and orbital angular momentum [2,4].

At variance with the single-photon regime, in the mesoscopic one the optical states contain many photons, thus resulting more robust against any external degradation [10–14]. Indeed, in a recent work of ours we have demonstrated that twin-beam (TWB) states of light preserve their nonclassicality even if one of the two parties propagates in a noisy and lossy channel [15]. Furthermore, we have shown that the calculation of the noise reduction factor makes the characterization of the transmission channel possible. Moreover, very recently we have proposed a novel quantum communication protocol [16] based on TWB states of light and the calculation of the noise reduction factor, in which the information is encoded in the noise superimposed to the TWB and the losses mimic an eavesdropper's interference.

Based on these successful results, here we consider a more realistic scenario, in which a portion of TWB, e.g. the signal, is sent through water-filled tubes, while the other portion, the idler, undergoes free-space propagation. In particular, we investigate the role played by the length of the tubes, the number of optical elements (OE) inserted in the setup, and the divergence of the beams through the two different media. We demonstrate that, by properly acting

#472034 https://doi.org/10.1364/OE.472034
Journal © 2022 Received 29 Jul 2022; revised 21 Sep 2022; accepted 3 Oct 2022; published 17 Nov 2022

Optics EXPRESS

on the light beams, we can still observe nonclassical correlations at moderate distances. The experimental implementations involve commercial photon-number-resolving (PNR) detectors. More specifically, hybrid photodetectors [17,18] and Silicon Photomultipliers [19,20] have been used and compared.

2. Model

Let's assume that the multi-mode TWB states we are dealing with are described by the density matrix [21]:

$$\rho_{\mathrm{TWB},\,\mu} = \sum_{n=0}^{\infty} P^{\mu}(n)|n,n\rangle\langle n,n|, \tag{1}$$

where $|n\rangle = \delta(n - \sum_{k=1}^{\mu} n_k) \bigotimes_{k=1}^{\mu} |n_k\rangle_k$ and n is the overall number of photons in the μ spatio-spectral modes that impinge on the detector, while $P^{\mu}(n)$ is the multi-mode thermal distribution

$$P^{\mu}(n) = \frac{(n+\mu-1)!}{n!(\mu-1)!\,(\langle n\rangle/\mu+1)^{\mu}\,(\mu/\langle n\rangle+1)^{n}}, \tag{2}$$

in which $\langle n\rangle$ is the mean number of photons in each arm. Such states are entangled in the number of photons. It has been already demonstrated that a sufficient criterion for entanglement can be given in terms of the noise reduction factor, which is defined as [22]

$$R = \frac{\sigma^2(n_1 - n_2)}{\langle n_1\rangle + \langle n_2\rangle}, \tag{3}$$

where $\sigma^2(n_1 - n_2)$ is the variance of the distribution of the photon-number difference between the two parties and $\langle n_1\rangle + \langle n_2\rangle$ is the so-called shot-noise level, that is the photon-number difference in the case of two coherent states having the same mean values as signal and idler. The condition $R<1$ indicates the existence of nonclassical correlations.

In some works of ours [23,24], we have demonstrated that the noise reduction factor can be also written in terms of detected photons, m. Moreover, we have shown that in the presence of an imbalance between signal and idler, and of a noise source in one TWB arm, R still attains an analytic form, that is [15]

$$R = 1 - \frac{2\eta t\langle m\rangle}{(1+t)\langle m\rangle + \langle m_{\mathrm{N}}\rangle} + \frac{(1-t)^2\langle m\rangle^2}{\mu\,[(1+t)\langle m\rangle + \langle m_{\mathrm{N}}\rangle]} + \frac{\sigma^2(m_{\mathrm{N}}) - \langle m_{\mathrm{N}}\rangle}{(1+t)\langle m\rangle + \langle m_{\mathrm{N}}\rangle}, \tag{4}$$

where $\langle m\rangle$ is the mean number of detected photons in a TWB arm, η is the global quantum efficiency of the detection system, t is transmission efficiency quantifying the balancing between signal and idler, while $\langle m_{\mathrm{N}}\rangle$ and $\sigma^2(m_{\mathrm{N}})$ are the mean value and the variance of the noise source, respectively.

Since such quantities explicitly appear in the expression of R, it is possible to estimate them from the fit of the experimental values of the noise reduction factor as a function of the mean value of light. This strategy allows us to completely characterize the transmission channel. In particular, we note that the coefficient t in Eq. (4) is used to take into account any kinds of loss and imbalance that can affect one arm with respect to the other one, also including all possible differences due to the use of a non-degenerate TWB state.

In the following, we consider the case in which the signal propagates through tubes filled with tap water, while the idler is transmitted in free space. For this kind of investigation we assume that the water in the tubes is static. Effects of water motion, such as turbulence, can be also included in the expression of the noise reduction factor, as already shown in Ref. [10]. If we assume that the main process affecting the propagation of light in water is absorption, the transmission efficiency t as a function of the propagation distance is described by $f(x) = 10^{-\alpha x}$, where α is the absorption

Optics EXPRESS

coefficient per unit length. In Fig. 1(a) we show the expected behavior for two different choices of the optical wavelength in the transmission window mentioned in the Introduction, namely in the blue-green region [25], in the case of clean water (Jerlov type I [26,27]). For different kinds of water the situation can be worse since the values of the transmission coefficient are definitely smaller, thus determining shorter propagation distances.

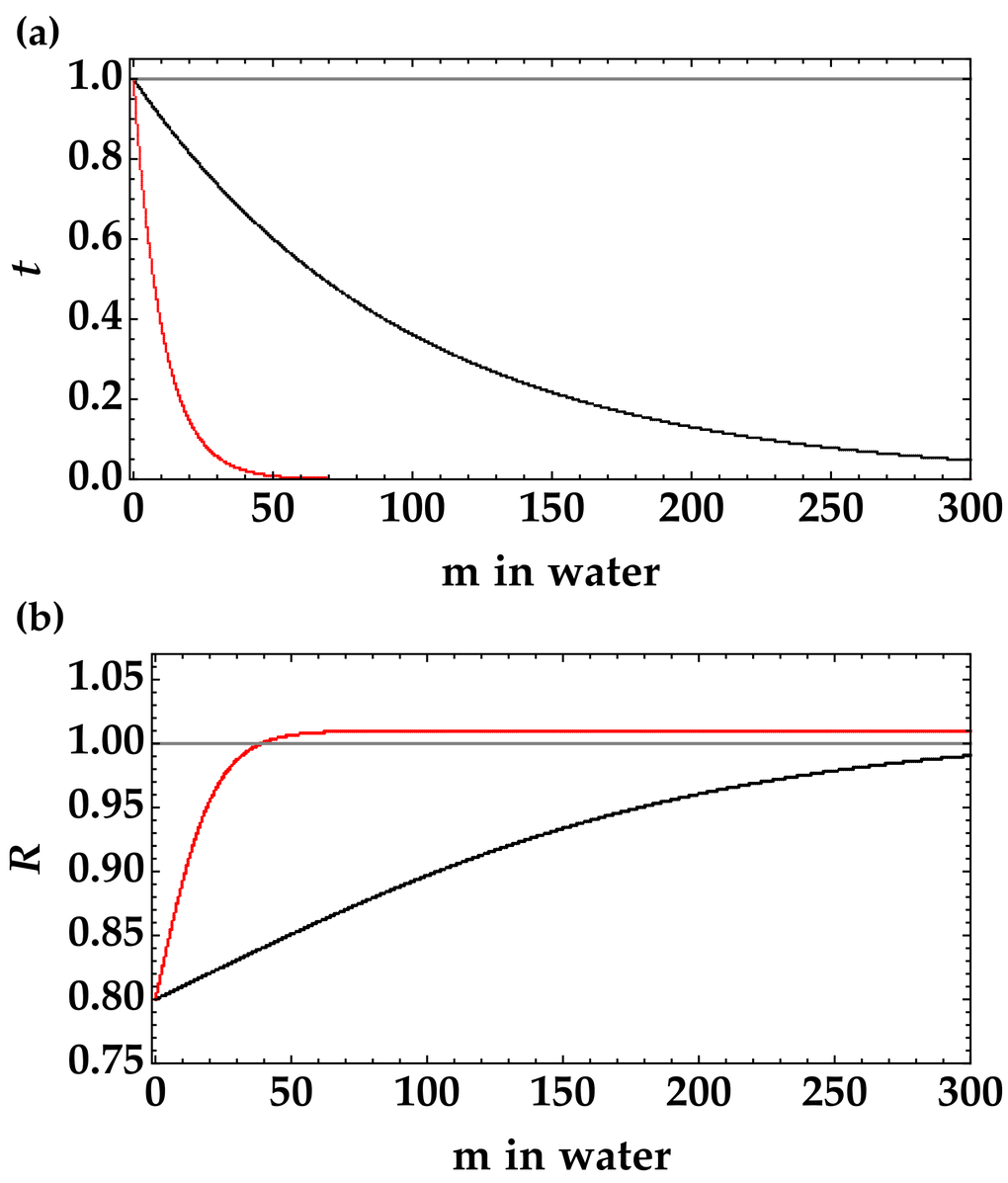

Fig. 1. (a) Transmission efficiency as a function of light propagation in water for $\lambda = 417.5$ nm (black curve) and $\lambda = 525$ nm (red curve) under the assumption of a pure absorption process. (b) Expected noise reduction factor as a function of the propagation in water for the same choices of wavelength as in panel (a). In this case we set $\eta = 0.2$, $\mu = 100$, $\langle m \rangle = 1$, $\langle m_{\mathrm{N}} \rangle = 0$, $\sigma^2(m_{\mathrm{N}}) = 0$. The value of α is 0.004 m^{-1} for $\lambda = 417.5$ nm and 0.041 m^{-1} for $\lambda = 525$ nm.

From Fig. 1(a) we can clearly see that for $\lambda = 417.5$ nm (the wavelength corresponding to the max transmittance) the propagation in water is allowed for a longer distance than for $\lambda = 525$ nm. For a fair comparison, in Fig. 1(b) we plot the expected behavior of R as a function of the propagation distance for the same choices of wavelength. The obtained results indicate that operating in the blue region is definitely better than in the green one, and would allow reaching the maximum distance while keeping sub-shot-noise correlations.

In view of performing a communication protocol in the real scenario, it is of crucial importance to characterize the transmission channel investigating the role played on the nonclassicality level by the different kinds of nonidealities affecting the transmission system. As better described in the following Section, we exploit the theoretical model in Eq. (4) to estimate the values corresponding to each drawback separately. As to the loss, we take into account the transmittance of the OE inserted in the path, the absorption of water passing through tubes with different lengths, and the natural divergence of the TWB. As to the noise, we consider the possible presence of dark counts, and of spurious light, such as the residual of infrared used to produce the pump beam.

Optics EXPRESS

3. Experimental results

The mesoscopic TWB states were generated by pumping a β-Barium-Borate (BBO) crystal with the fourth-harmonic pulses (262 nm) of a Nd:YLF laser regeneratively amplified at 500 Hz. Even if, according to Fig. 1, the best solution for an optimal propagation in water should be the selection of a signal wavelength in the blue region, for the different kinds of characterizations presented in the following we chose to work at frequency degeneracy, that is at 523 nm, in order to match the maximum quantum efficiency of the adopted PNR detectors and to consider it equal in the two arms.

The two portions at frequency degeneracy were spectrally selected by means of band-pass filters, focused into two multi-mode fibers with 600-μm core diameter and delivered to the photodetectors. As to the detectors, we considered two classes of commercial PNR detectors. In more detail, we used a pair of hybrid photodetectors (HPD, mod. R10467U-40, Hamamatsu Photonics) kept at 16°C for almost all the characterizations, while in the final part of the work we compared the results obtained with HPDs with those corresponding to a pair of Silicon Photomultipliers (SiPM, mod. MPPC S13360-1350CS, Hamamatsu Photonics). In both cases, the two detector outputs were amplified by shaping amplifiers, synchronously integrated by means of boxcar-gated integrators (SR250, Stanford), and digitized (PCI-6251, National Instruments). By applying the self-consistent method already explained elsewhere [17,28,29], we converted the output voltages into numbers of detected photons and thus calculated all the relevant statistical quantities, such as the noise reduction factor, in terms of measurable quantities [23,24,30].

For all the characterizations, we performed measurements as a function of the mean value of TWB. To this aim, the energy of the pump field was changed in steps by means of a half-wave plate followed by a polarizing cube beam splitter. For each mean value of the pump, 100,000 acquisitions were recorded.

The first kind of characterization is aimed at investigating how the nonclassicality of TWB states is modified by the propagation of the signal in water over short distances. In this case, the collection of light was performed at $\sim$ 80 cm from the BBO, and the tubes filled with tap water used in the signal arm were 30-cm, 40-cm, and 60-cm long. A pair of BK7 laser windows was used to maintain the water inside each tube. The typical setup is shown in panel (a) of Fig. 2, while pictures of the tubes and of the mounts of the OE are presented in panels (b) and (c), respectively. In Fig. 3(a) we show the noise reduction factor as a function of the mean number of detected photons in one TWB arm, from which it is well clear that in all the investigated cases it is still possible to observe nonclassical correlations between the two parties. The black dots correspond to the measurements in the absence of tubes, while the red, blue, and green dots correspond to the presence of a tube with a length of 30 cm, 40 cm and 60 cm, respectively, placed in the signal arm, close to the collection of light. Each data set is well superimposed to the theoretical expectation, in which the values of the possible losses and noise sources were extracted as free parameters from the fitting function according to Eq. (4), while μ was obtained as fitting parameter from the reconstructed distributions of detected photons. Concerning the values, which are summarized in panel (b) of Fig. 3, we can notice that the transmittance decreases at larger values of the length of tubes. On the contrary, the noise contribution, under the assumption that it is Poissonian, is almost constant, so that it should be ascribed to the presence of dark counts. In the following, we will exploit the values of t to extract information about the loss due to water absorption.

The second kind of characterization is aimed at evaluating the loss due to the number of OE introduced in the signal arm with respect to the idler one. Indeed, such a characterization is crucial in order to isolate the loss contribution due to water absorption presented in the following. In this case, we kept fixed the length of the transmission channel in water, and used one, two, and three tubes. In particular, we used a 60-cm-long tube, a 20-cm-long tube + a 40-cm-long one, and a 10-cm-long BK7 cell + a 20-cm-long tube + a 30-cm-long one. The employed setup is still sketched in Fig. 2(a), while the noise reduction factor as a function of the mean value of a

Optics EXPRESS

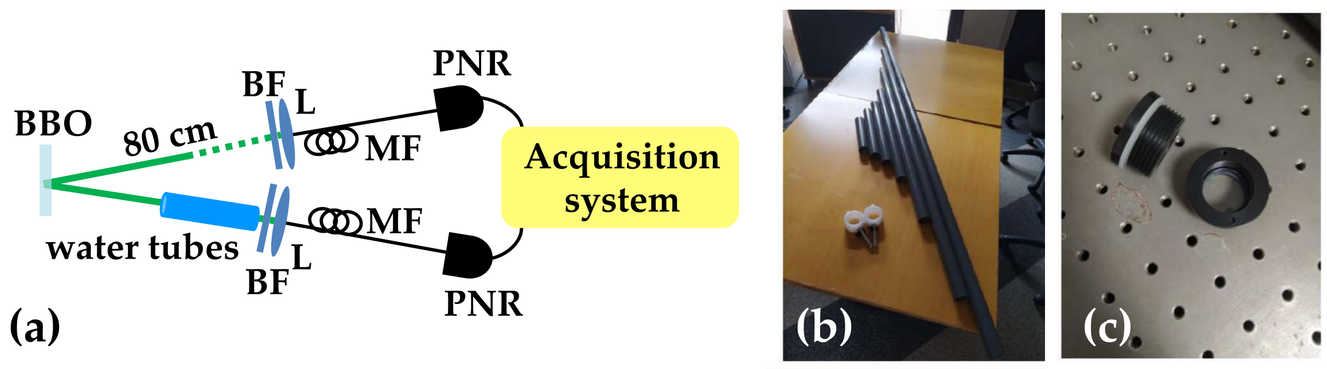

Fig. 2. (a) Sketch of the experimental setup for the first and second kinds of characterization; (b) Picture of the PVC tubes; (c) Picture of the mounts of the OE. See the text for details.

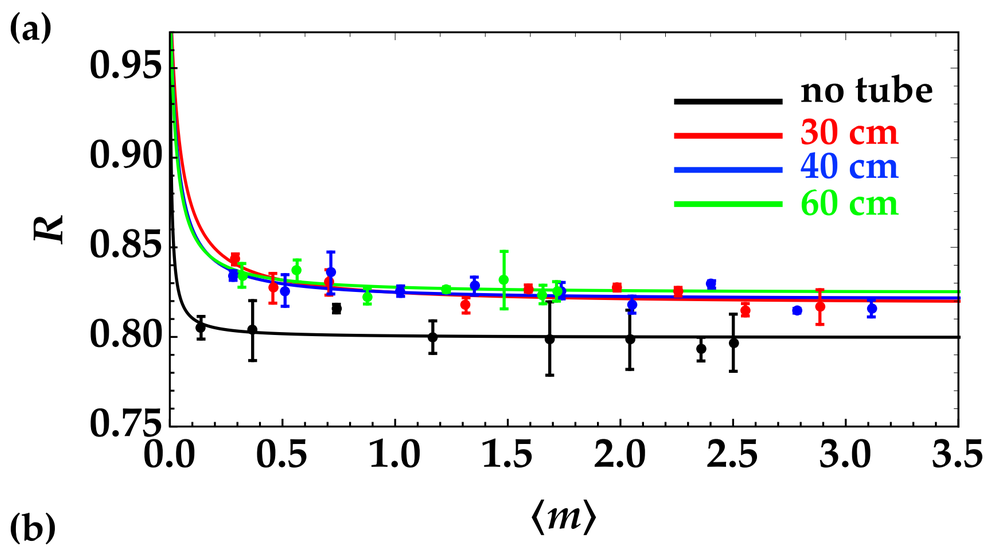

(b)

	No tube	30 cm	40 cm	60 cm
t	1	0.84 ± 0.03	0.82 ± 0.03	0.79 ± 0.04
$\langle m_N \rangle$	0.01 ± 0.02	0.08 ± 0.03	0.05 ± 0.03	0.04 ± 0.04

Fig. 3. (a) Noise reduction factor as a function of the mean number of detected photons in a TWB arm in the case in which a tube filled with water is inserted in the signal arm. Black dots: no tube; red dots: 30-cm-long tube; blue dots: 40-cm-long tube; green dots: 60-cm-long tube. For each case, the theoretical fitting function according to Eq. (4) is shown with the same color choice. (b) Values of the fitting parameters t and $\langle m_N \rangle$ for the four cases plotted in panel (a) and using the fitting parameter $\eta = 0.200 \pm 0.004$ obtained in the absence of tubes. Note that in the case "No tube" t has been considered equal to 1.

TWB arm is shown in Fig. 4(a). The black dots correspond to the case of a single tube, the red dots to two tubes, and the blue dots to three tubes. As in the case of the first characterization, we still observe nonclassical correlations, even if the absolute values of R are worse due to the number of OE inserted in the signal arm. In particular, the larger the number the higher the value of R. From the fitting functions of the three cases (see Fig. 4(b)) and considering the information about the detection efficiency obtained from the fit of the black dots in Fig. 3, we can extract information about the transmittance coefficient of a single OE. Indeed, by considering the case of a single tube, in which there are two OE, and the remaining two cases, with four and six OE respectively, we obtain $t_{OE} = \sqrt{0.62/0.79} = 0.89$ and $t_{OE} = \sqrt[4]{0.60/0.79} = 0.93$. By considering the error propagations, the two values become: $t_{OE} = 0.89 \pm 0.05$ and $t_{OE} = 0.93 \pm 0.06$, which are in excellent agreement with the results of absorption measurements taken by means of a spectrophotometer, that is $t = 0.92 \pm 0.01$.

Thanks to these successful results, in the following we show the third kind of investigation, that is the propagation of light in water over a longer distance. In this case, the signal covered an overall distance of 252 cm, 170 of which were in water, whereas the idler covered a global distance 201-cm long in free-space. The sketch of the corresponding experimental setup is shown

Optics EXPRESS

(a)

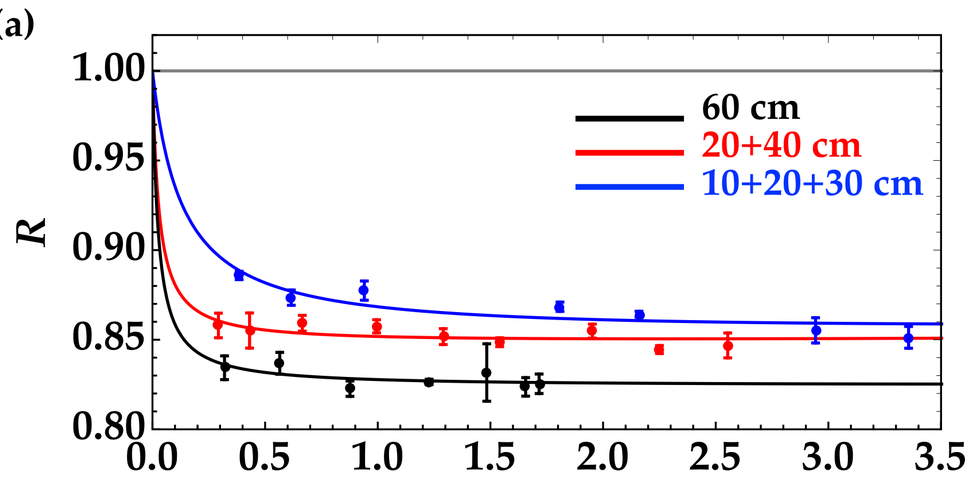

(b)

	60 cm	20+40 cm	10+20+30 cm
t	0.79 ± 0.04	0.62 ± 0.02	0.60 ± 0.04
$<m_N>$	0.04 ±0.04	0.05 ±0.03	0.21 ± 0.09

Fig. 4. (a) Noise reduction factor as a function of the mean number of detected photons in a TWB arm in the case in which one or more tubes filled with water are inserted in the signal arm. Black dots: 60-cm-long tube; red dots: 20-cm-long tube + 40-cm-long one; blue dots: 10-cm BK7 cell + 20-cm-long tube + 30-cm-long one. For each case, the theoretical fitting function according to Eq. (4) is shown with the same color choice. (b) Values of the fitting parameters t and $\langle m_N \rangle$ for the three cases plotted in panel (a) and using the fitting parameter $\eta = 0.200 \pm 0.004$ obtained in the absence of tubes.

in Fig. 5(a), while a picture of the optical table is shown in panel (b) of the same figure. We note that, apart from the presence of tubes, the two arms are quite similar. In particular, in both arms we introduced a lens with a 1-m focal length to collimate the two twin portions. Each lens was located at a distance of 1 m from the collection system. Because of the space at our disposal on the optical table, the propagation in water was obtained by means of three tubes (30-cm, 40-cm and 1-m long) rather than in a single one. According to the sketch of the experimental setup in Fig. 5(a), two laser windows were substituted by two 2-m-focal-length lenses. It is remarkable that this choice allows us to better keep under control the divergence of the beam. In order to evaluate the possible loss sources separately, we calculated the noise reduction factor under three different conditions, that is with the tubes without OE and water, with the tubes and the OE but without water, and finally with the tubes filled with water. In Fig. 6(a) we show the noise reduction factor as a function of the mean value in a TWB arm for the three conditions. We note that in all cases we still observe nonclassical correlations. Moreover, from the fit of the data (see Fig. 6(b) for a summary) we can extract useful information about losses. For instance, we can compare the values of t in the presence and in the absence of OE, from which we obtain again the typical transmittance value of a lens or of a laser window. In particular, we obtain $t_{OE} = \sqrt[6]{0.536/0.944} = 0.932$. By also propagating the errors, the value of the transmission coefficient per OE is $t_{OE} = 0.93 \pm 0.05$, which is in good agreement with the results of absorption measurements taken by means of a spectrophotometer, as mentioned above. Furthermore, by comparing the values of t in the presence and in the absence of water we can extract information about the absorption of water itself, that is $t_w = 0.455/0.536 = 0.848$. After evaluating the error, we get $t_w = 0.85 \pm 0.05$. By comparing this value with those obtained in the first kind of investigation (see panel (b) of Fig. 3) divided by the loss introduced by two laser windows (0.92^2), we can study the loss due to water absorption. The data are shown in Fig. 7 as black dots, while the theoretical fitting function $f(x) = 10^{-\alpha x}$, where α is the absorption coefficient per unit length, is shown as red curve. From the fit we obtained $\alpha = 0.04 \pm 0.01$ m^{-1}, which is in perfect agreement with the value reported on the literature [25].

Optics EXPRESS

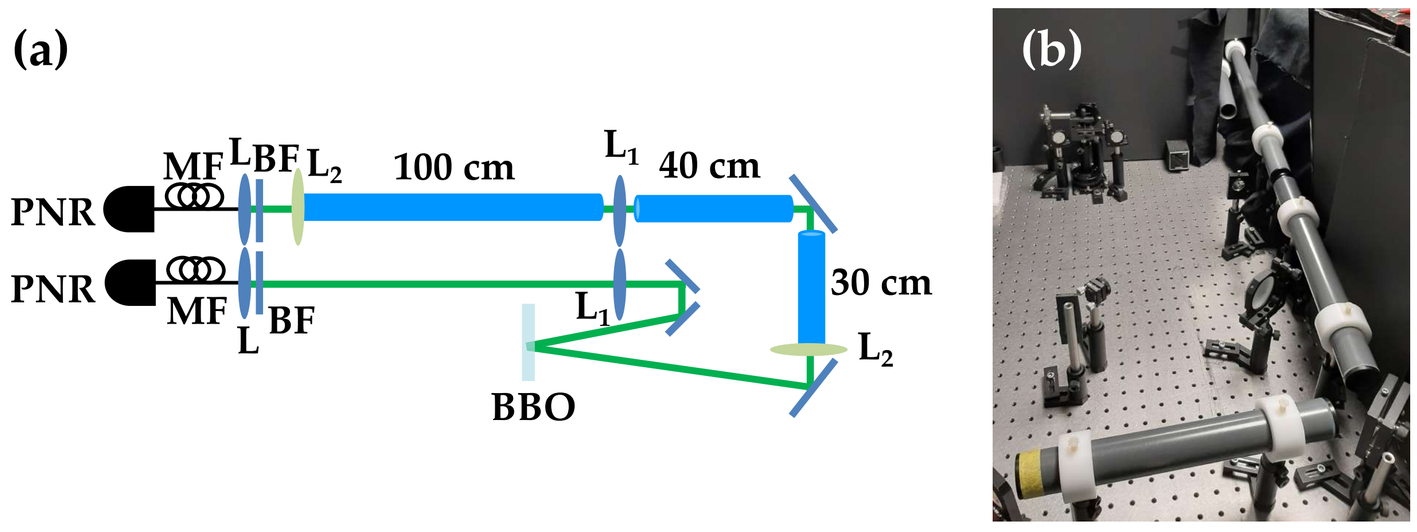

Fig. 5. (a) Sketch of the experimental setup for the third kind of characterization, in which L_1 = 1-m focal-length lens and L_2 = 2-m focal-length lens; (b) Picture of the optical table. See the text for details.

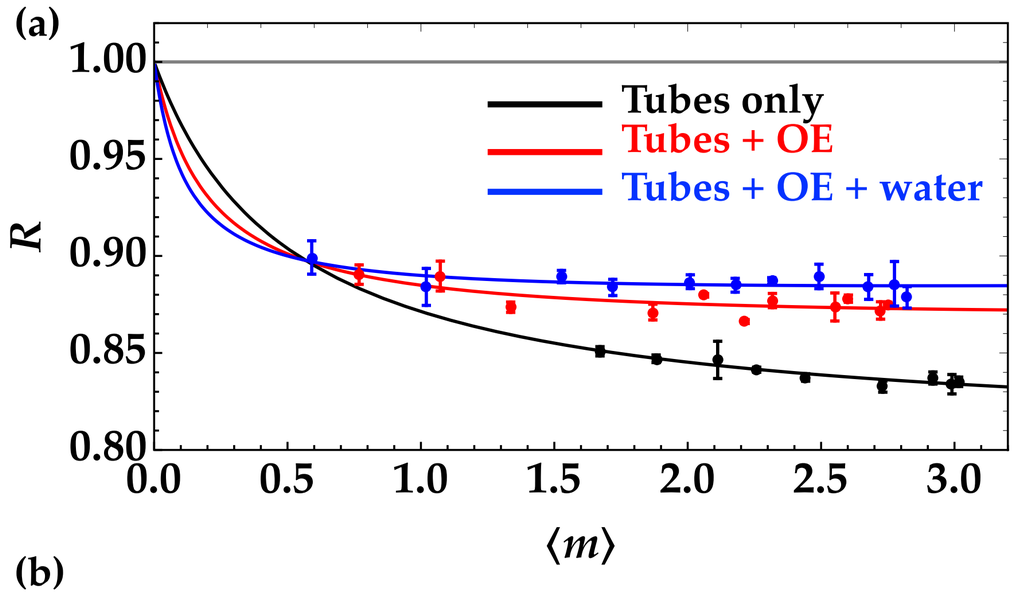

(b)

	Tubes only	Tubes + OE	Tubes + OE + water
t	0.94 ± 0.07	0.54 ± 0.03	0.45 ± 0.01
$<m_N>$	1.0 ± 0.2	0.3 ± 0.1	0.18 ± 0.06

Fig. 6. (a) Noise reduction factor as a function of the mean number of detected photons in a TWB arm for a propagation in water 170-cm long. Black dots: tubes without OE and water; red dots: tubes with OE and without water; blue dots: tubes with OE and water. For each case, the theoretical fitting function according to Eq. (4) is shown with the same color choice. (b) Values of the fitting parameters t and $\langle m_N \rangle$ for the three cases plotted in panel (a) and using the fitting parameter $\eta = 0.200 \pm 0.004$ obtained in the absence of tubes.

Optics EXPRESS

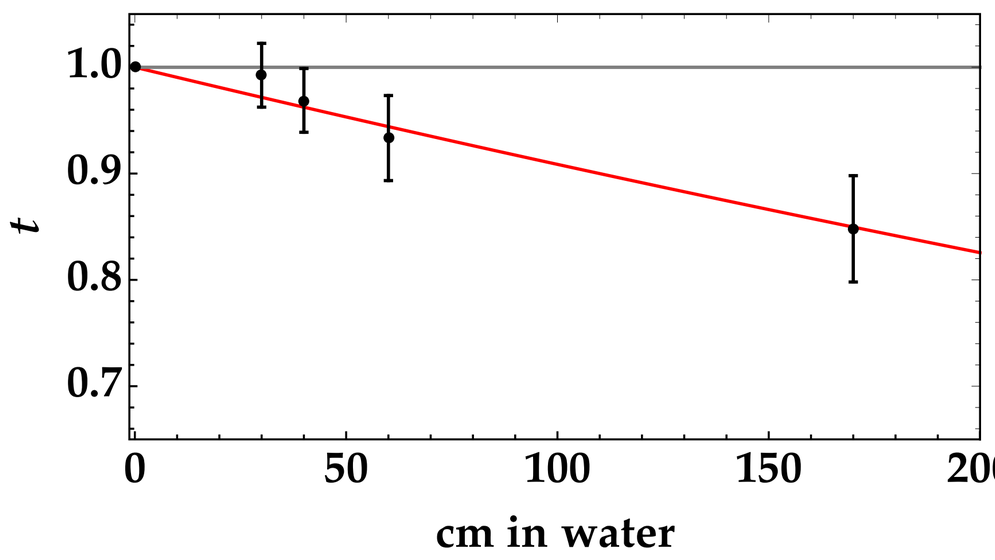

Fig. 7. Values of t as a function of light propagation in water. Black dots: experimental data; red curve: theoretical fitting function $f(x) = 10^{-\alpha x}$, where α is the absorption coefficient per unit length. The obtained fitting parameter is $\alpha = 0.04 \pm 0.01$ m^{-1}.

As a final investigation, for the setup in Fig. 5(a) we also consider the possibility to detect the two light portions with a different class of PNR detectors, that is with a pair of SiPMs. These are PNR detectors characterized by hundreds of pixels (or cells) operated in the Geiger–Müller regime and read in parallel, in order to yield a single output [31–35]. As already explained in [20], these two detectors were amplified by means of a home-made circuit including a slow non-inverting amplifier with two amplifying stages [25], each one having a gain of 5.5 for a total gain of 29.6 dB. The amplified outputs were integrated over a gate 50-ns long by means of two boxcar-gated integrators and acquired. SiPMs are endowed with an excellent PNR capability [36], as shown in Fig. 8, where the pulse-height spectra of HPDs and SiPMs are directly compared. The comparison of the results about the noise reduction factor obtained by means of HPDs and SiPMs is shown in Fig. 9(a), while the values of the fitting parameters are presented in panel (b) of the same figure. We can clearly see that the values of R as a function of the mean value in a TWB arm are definitely worse in the case of SiPMs. This fact can be probably ascribed to a non-perfect coupling between the optical fiber and the SiPM sensor. Indeed, only if we are operatig under the condition in which each cell is fired by at most one photon, the number of fired cells should correspond to the number of impinging photons. Moreover, SiPMs were used at room temperature, and by lowering the temperature their quantum efficiency may be increased. By improving these aspects, better results could be achieved. Furthermore, we notice that from the experimental point of view the use of SiPMs required a strongest shielding apparatus because of the diffused infrared light to which for instance the employed optical fiber resulted transparent. Despite these drawbacks the use of SiPMs as the PNR detectors is highly desirable since they are compact, cheap and portable with respect to HPDs. Moreover, they have a larger dynamic range, up to tens of photons, so that they are useful to detect well-populated optical states. Thus, further improvements are now needed in view of exploiting the detection apparatus in the real scenario.

Optics EXPRESS

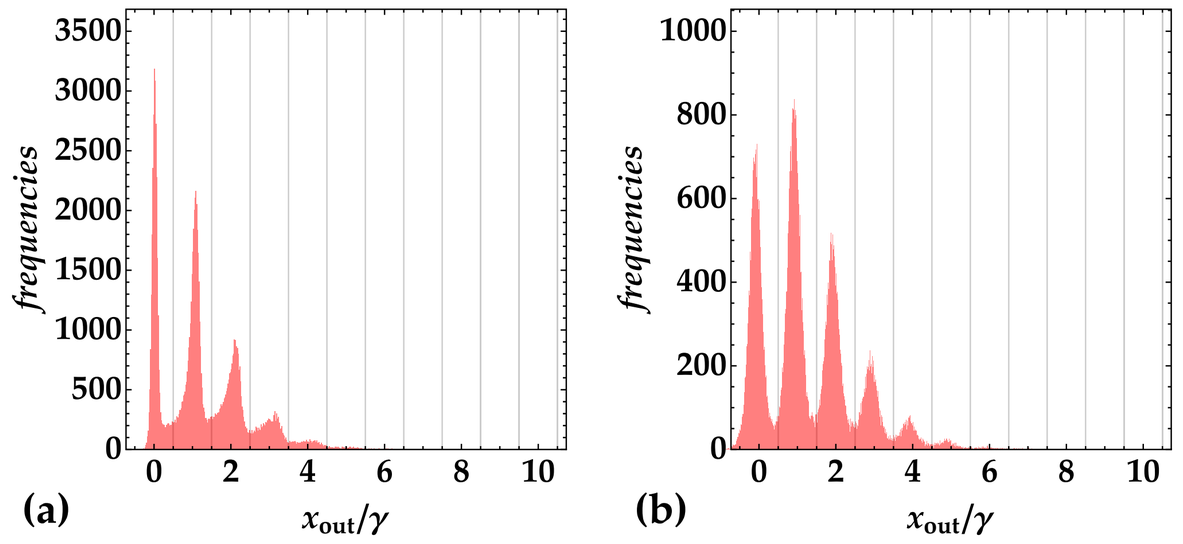

Fig. 8. Typical pulse-height spectra of HPD (panel (a)) and of SiPM (panel (b)). In both cases the mean value of the light is $\langle m \rangle \sim 1.3$.

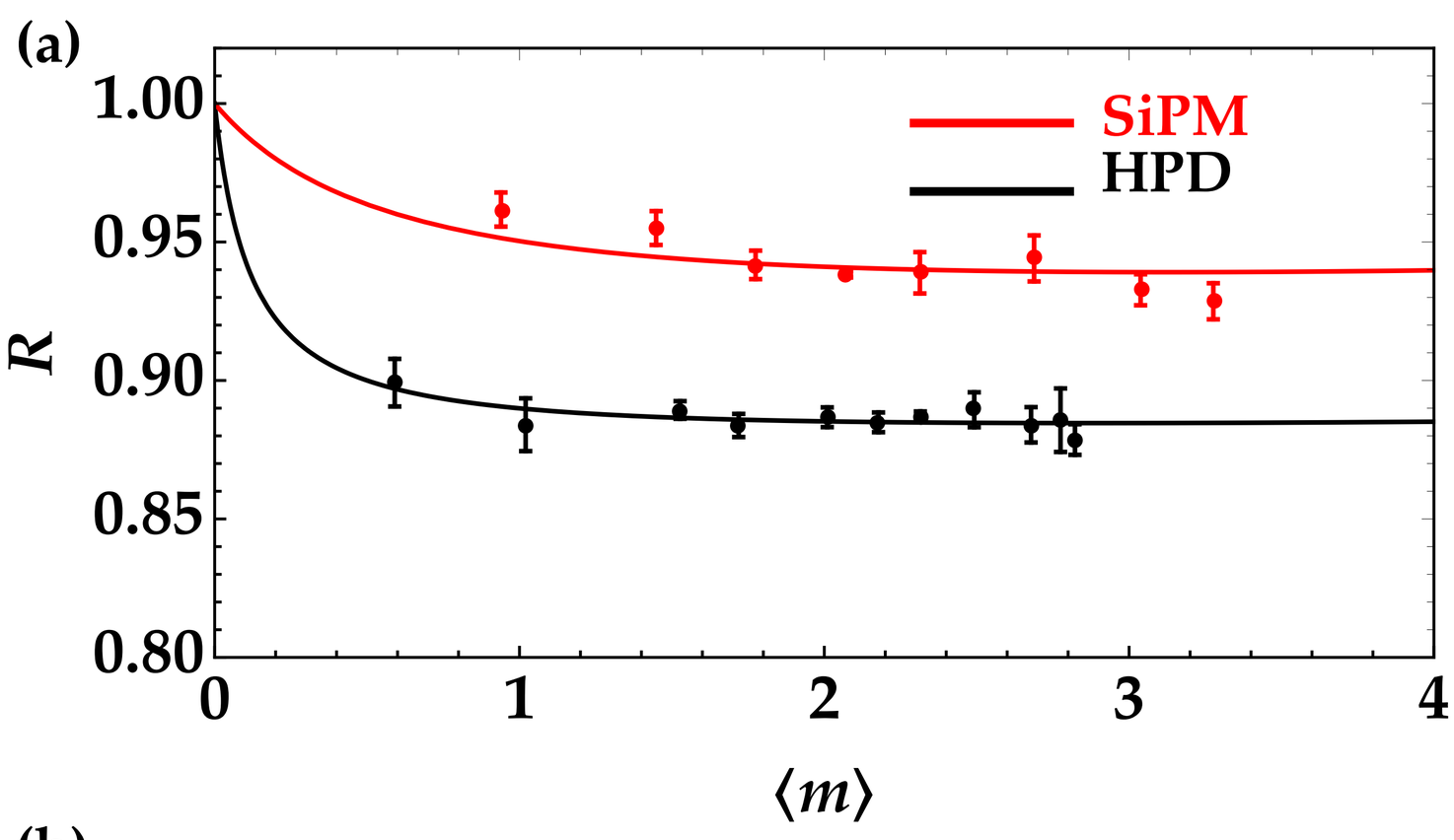

(b)

	HPD	SiPM
η	0.200 ± 0.004	0.14 ± 0.03
$<m_N>$	0.18 ± 0.06	1.0 ± 0.9

Fig. 9. (a) Noise reduction factor as a function of the mean number of detected photons in a TWB arm for a propagation in water 170-cm long. Black dots: data obtained using HPDs; red dots: data obtained using SiPMs. For each case, the theoretical fitting function according to Eq. (4) is shown with the same color choice. (b) Values of the fitting parameters η and $\langle m_N \rangle$ obtained detecting light with HPDs or SiPMs for t=0.455.

Optics EXPRESS

4. Conclusions

In this paper, we tested the robustness of mesoscopic TWB states propagating partly in free space and partly in tubes filled with water. On the one hand, we demonstrated that the quantum states remain nonclassical even in the presence of different kinds of loss and noise sources. On the other hand, we used the nonclassicality criterion based on the noise reduction factor to extract information about these loss and noise sources. The values obtained as fitting parameters are in perfect agreement with those reported on the literature and on datasheet, thus proving the goodness of the method. In the final part of the work, we also compared the results obtained with HPDs and SiPMs. Currently, the latter ones are worse than the others. However, SiPMs present many advantages such as cheapness, compactness, and portability. Thus, as discussed in the final part of the work, they deserve further improvements, such as a temperature control and a better fiber-to-sensor coupling. Indeed, these tricks can open new perspectives in the real employment of mesoscopic states of light and PNR detectors for the implementation of novel underwater quantum communication protocols. Finally, we plan to better investigate how to control the divergence of the beams in a more realistic scenario by considering the free propagation in a tank filled with water rather than in tubes. To this aim, we could manage to spatially manipulate the beams in order to make them more collimated over a longer distance.

Acknowledgments. A. A. acknowledges the Project "Investigating the effect of noise sources in the free-space transmission of mesoscopic quantum states of light" supported by the University of Insubria.

Disclosures. The authors declare no conflicts of interest.

Data availability. Data underlying the results presented in this paper are not publicly available at this time but may be obtained from the authors upon reasonable request.

References

1. D. Cozzolino, B. Da Lio, D. Bacco, and L. K. Oxenløwe, "High-dimensional Quantum Communication: Benefits, progress, and future challenges," Adv. Quantum Technol. **2**(12), 1900038 (2019).
2. L. Ji, J. Gao, A.-L. Yang, Z. Feng, X.-F. Lin, Z.-G. Li, and X.-M. Jin, "Towards quantum communications in free-space seawater," Opt. Express **25**(17), 19795–19806 (2017).
3. C.-Q. Hu, Z.-Q. Yan, J. Gao, Z.-Q. Jiao, Z.-M. Li, W.-G. Shen, Y. Chen, R.-J. Ren, L.-F. Qiao, A.-L. Yang, H. Tang, and X.-M. Jin, "Transmission of photonic polarization states through 55-m water: towards air-to-sea quantum communication," Photonics Res. **7**(8), A40 (2019).
4. F. Hufnagel, A. Sit, F. Grenapin, F. Bouchard, K. Heshami, D. England, Y. Zhang, B. J. Sussman, R. W. Boyd, G. Leuchs, and E. Karimi, "Characterization of an underwater channel for quantum communications in the Ottawa River," Opt. Express **27**(19), 26346 (2019).
5. S. Zhao, W. Li, Y. Shen, Y.-H. Yu, X.-H. Han, H. Zeng, M. Cai, T. Qian, S. Wang, Z. Wang, Y. Xiao, and Y. Gu, "Experimental investigation of quantum key distribution over a water channel," Appl. Opt. **58**(14), 3902–3907 (2019).
6. S. A. Sullivan, "Experimental Study of the Absorption in Distilled Water, Artificial Sea Water, and Heavy Water in the Visible Region of the Spectrum," J. Opt. Soc. Am. **53**(8), 962 (1963).
7. F. Flamini, N. Spagnolo, and F. Sciarrino, "Photonic quantum information processing: a review," Rep. Prog. Phys. **82**(1), 016001 (2019).
8. Z. Zeng, S. Fu, H. Zhang, Y. Dong, and J. Cheng, "A survey of underwater optical wireless communications," IEEE Commun. Surv. Tutorials **19**(1), 204–238 (2017).
9. F. Hufnagel, A. Sit, F. Bouchard, Y. Zhang, D. England, K. Heshami, B. J. Sussman, and E. Karimi, "Investigation of underwater quantum channels in a 30 meter flume tank using structured photons," New J. Phys. **22**(9), 093074 (2020).
10. A. Allevi and M. Bondani, "Preserving nonclassical correlations in strongly unbalanced conditions," J. Opt. Soc. Am. B **36**(12), 3275–3281 (2019).
11. A. Allevi and M. Bondani, "Tailoring asymmetric lossy channels to test the robustness of mesoscopic quantum states of light," Appl. Sci. **10**(24), 9094 (2020).
12. J. Peřina Jr., I. I. Arkhipov, V. Michálek, and O. Haderka, "Nonclassicality and entanglement criteria for bipartite optical fields characterized by quadratic detectors," Phys. Rev. A **96**(4), 043845 (2017).
13. J. Peřina Jr., V. Michálek, and O. Haderka, "Nonclassicality and entanglement criteria for bipartite optical fields characterized by quadratic detectors. II. Criteria based on probabilities," Phys. Rev. A **102**(4), 043713 (2020).
14. V. Michálek, J. Peřina Jr., and O. Haderka, "Experimental Quantification of the Entanglement of Noisy Twin Beams," Phys. Rev. Appl. **14**(2), 024003 (2020).
15. A. Allevi and M. Bondani, "Effect of noisy channels on the transmission of mesoscopic twin-beam states," Opt. Express **29**(21), 32842–32852 (2021).

Optics EXPRESS

16. A. Allevi and M. Bondani, "Novel scheme for secure data transmission based on mesoscopic twin beams and photon-number-resolving detectors," Sci. Rep. **12**(1), 15621 (2022).
17. M. Bondani, A. Allevi, A. Agliati, and A. Andreoni, "Self-consistent characterization of light statistics," J. Mod. Opt. **56**(2-3), 226–231 (2009).
18. A. Allevi and M. Bondani, "Nonlinear and quantum optical properties and applications of intense twin-beams," Adv. At. Mol. Opt. Phys. **66**, 49–110 (2017).
19. G. Chesi, L. Malinverno, A. Allevi, R. Santoro, M. Caccia, and M. Bondani, "Measuring nonclassicality with silicon photomultipliers," Opt. Lett. **44**(6), 1371–1374 (2019).
20. S. Cassina, A. Allevi, V. Mascagna, M. Prest, E. Vallazza, and M. Bondani, "Exploiting the wide dynamic range of silicon photomultipliers for quantum optics applications," EPJ Quantum Technol. **8**(1), 4 (2021).
21. A. Allevi and M. Bondani, "Multi-mode twin-beam states in the mesoscopic intensity domain," Phys. Lett. A **423**, 127828 (2022).
22. A. Agliati, M. Bondani, A. Andreoni, G. De Cillis, and M. G. A. Paris, "Quantum and classical correlations of intense beams of light investigated via joint photodetection," J. Opt. B: Quantum Semiclassical Opt. **7**(12), S652–S663 (2005).
23. M. Bondani, A. Allevi, G. Zambra, M. G. A. Paris, and A. Andreoni, "Sub-shot-noise photon-number correlation in a mesoscopic twin beam of light," Phys. Rev. A **76**(1), 013833 (2007).
24. A. Allevi, S. Olivares, and M. Bondani, "Measuring high-order photon-number correlations in experiments with multimode pulsed quantum states," Phys. Rev. A **85**(6), 063835 (2012).
25. R. M. Pope and E. S. Fry, "Absorption spectrum (380–700 nm) of pure water. II. Integrating cavity measurements," Appl. Opt. **36**(33), 8710–8723 (1997).
26. M. G. Solonenko and C. D. Mobley, "Inherent optical properties of Jerlov water types," Appl. Opt. **54**(17), 5392–5401 (2015).
27. Z. Feng, S. Li, and Z. Xu, "Experimental underwater quantum key distribution," Opt. Express **29**(6), 8725–8736 (2021).
28. M. Bondani, A. Allevi, and A. Andreoni, "Light Statistics by Non-Calibrated Linear Photodetectors," Adv. Sci. Lett. **2**(4), 463–468 (2009).
29. A. Allevi and M. Bondani, "Statistics of twin-beam states by photon-number resolving detectors up to pump depletion," J. Opt. Soc. Am. B **31**(10), B14–B19 (2014).
30. J. Peřina Jr., O. Haderka, A. Allevi, and M. Bondani, "Absolute calibration of photon-number-resolving detectors with an analog output using twin beams," Appl. Phys. Lett. **104**(4), 041113 (2014).
31. A. V. Akindinov, A. N. Martemianov, P. A. Polozov, V. M. Golovin, and E. A. Grigoriev, "New results on MRS APDs," Nucl. Instrum. Methods Phys. Res., Sect. A **387**(1-2), 231–234 (1997).
32. G. Bondarenko, B. Dolgoshein, V. Golovin, A. Ilyin, R. Klanner, and E. Popova, "Limited Geiger-mode silicon photodiode with very high gain," Nucl. Phys. B, Proc. Suppl. **61**(3), 347–352 (1998).
33. V. Saveliev and V. Golutvin, "Silicon avalanche photodiodes on the base of metal-resistor-semiconductor (MRS) structures," Nucl. Instrum. Methods Phys. Res., Sect. A **442**(1-3), 223–229 (2000).
34. C. Piemonte, "A new Silicon Photomultiplier structure for blue light detection," Nucl. Instrum. Methods Phys. Res., Sect. A **568**(1), 224–232 (2006).
35. D. Renker and E. Lorenz, "Advances in solid state photon detectors," J. Instrum. **4**(04), P04004 (2009).
36. R. Klanner, "Characterisation of SiPMs," Nucl. Instrum. Methods Phys. Res., Sect. A **926**, 36–56 (2019).